Improvement of the female mouse computational model developed at CDTN

Aprimoramento do modelo computacional do camundongo fêmea desenvolvido no CDTN

DOI:10.34117/bjdv9n5-031

Recebimento dos originais: 04/04/2023
Aceitação para publicação: 04/05/2023

Joana D'Arc Souza Rodrigues
Graduanda em Ciências Biológicas
Instituição: Centro de Desenvolvimento da Tecnologia Nuclear (CDTN)
Endereço: Campus da Universidade Federal de Avenida Presidente Antônio Carlos, Rua Mário Werneck, S/N, Pampulha, Belo Horizonte - MG, CEP: 31270-901
E-mail: Joanadsr2323@gmail.com

Bruno Melo Mendes
Doutor em Ciências Biológicas
Instituição: Centro de Desenvolvimento da Tecnologia Nuclear (CDTN)
Endereço: Campus da Universidade Federal de Avenida Presidente Antônio Carlos, Rua Mário Werneck, S/N, Pampulha, Belo Horizonte - MG, CEP: 31270-901

Christiane Silva Leite
Graduanda em Ciências Biológicas
Instituição: Centro de Desenvolvimento da Tecnologia Nuclear (CDTN)
Endereço: Campus da Universidade Federal de Avenida Presidente Antônio Carlos, Rua Mário Werneck, S/N, Pampulha, Belo Horizonte - MG, CEP: 31270-901

Ana Carolina de Araujo Bispo
Doutora em Farmácia
Instituição: Centro de Desenvolvimento da Tecnologia Nuclear (CDTN)
Endereço: Campus da Universidade Federal de Avenida Presidente Antônio Carlos, Rua Mário Werneck, S/N, Pampulha, Belo Horizonte - MG, CEP: 31270-901

Andrea Vidal Ferreira
Doutora em Física
Instituição: Centro de Desenvolvimento da Tecnologia Nuclear (CDTN)
Endereço: Campus da Universidade Federal de Avenida Presidente Antônio Carlos, Rua Mário Werneck, S/N, Pampulha, Belo Horizonte - MG, CEP: 31270-901

Juliana Batista Silva
Doutora em Química
Instituição: Centro de Desenvolvimento da Tecnologia Nuclear (CDTN)
Endereço: Campus da Universidade Federal de Avenida Presidente Antônio Carlos, Rua Mário Werneck, S/N, Pampulha, Belo Horizonte - MG, CEP: 31270-901

Anne Roivainen
PhD Medicina
Instituição: Institute of Biomedicine University of Turku
Endereço: FI-20014 Turun yliopisto, Finland

Teuho Jarmo
Doutor em Física Médica e Engenharia pela Universidade Turku
Instituição: Institute of Biomedicine University of Turku
Endereço: FI-20014 Turun yliopisto, Finland

ABSTRACT
Small animals, such as mice, have been used in experiments involving ionizing radiation. New preclinical experimental methods often include extensive imaging (MicroCT and/or PET/SPECT) that can result in absorbed dose values considerably high. In addition, assays with theranosticsradiopharmaceuticals administered in small animals have been used to determine the main potential adverse effects and the therapeutic efficacy. For all these mentioned cases, the precise quantification of absorbed doses and the determination of energy deposition patterns are of fundamental importance to qualify or exclude potential radiobiological effects that may interfere with in vivo experiment results. Thus, the development and improvement of mouse phantoms is essential for good small animal dosimetry. In 2021, our group segmented and implemented a female C57BL mouse phantom, called FM_BRA, in the MCNP. The objective of this work was to review the segmentation of the FM_BRA computational model and to identify and segment new organs for an improved version of this phantom. Three different researchers segmented different organs of the model. The masses of the segmented organs were compared with those of the first version. Information on mass or volume of organs from different mouse strains, and more specifically from the C57BL strain, was also obtained from the literature for comparison and to aid in segmentation. The mice image representing a female mouse of the C57BL strain weighing 26 g were kindly provided by the Turku Center for Disease and were manually segmented. The software GIMP® 2.10 was used to select and segment each organ/tissue. The IMAIOS-VET Anatomy website was used as an anatomical basis for the identification of organs/tissues. The IMAGEJ® software was applied to assemble the segmented images into a 3D stack and to convert the segmented images into binary files. The volumes of the segmented organs were measured with a C^{++} in house program. Corresponding human tissue densities provided in ICRP 110 were used to calculate organ mass from the calculated volumes. Data were compared with literature reports. The number of segmented organs increased from 20 in the old model to 33 in the new models. The masses of the organs segmented in this work, by the different researchers, showed agreement in most cases. However, organs such as the small intestines, bones and trachea still deserve a new round of reviewing.

Keywords: dosimetry, mouse phantoms, computational model, segmentation.

RESUMO

Pequenos animais, como camundongos, têm sido usados em experimentos que envolvem radiação ionizante. Os novos métodos experimentais pré-clínicos geralmente incluem imagens extensas (MicroCT e/ou PET/SPECT) que podem resultar em valores de dose absorvida consideravelmente altos. Além disso, ensaios com teranósticos radiofármacos administrados em pequenos animais têm sido usados para determinar os principais efeitos adversos potenciais e a eficácia terapêutica. Em todos esses casos mencionados, a quantificação precisa das doses absorvidas e a determinação dos padrões de deposição de energia são de fundamental importância para qualificar ou excluir possíveis efeitos radiobiológicos que possam interferir nos resultados dos experimentos in vivo. Assim, o desenvolvimento e o aprimoramento de fantomas de camundongos são essenciais para uma boa dosimetria de pequenos animais. Em 2021, nosso grupo segmentou e implementou um fantoma de camundongo C57BL fêmea, denominado FM_BRA, no MCNP. O objetivo deste trabalho foi revisar a segmentação do modelo computacional FM_BRA e identificar e segmentar novos órgãos para uma versão aprimorada desse fantoma. Três pesquisadores diferentes segmentaram diferentes órgãos do modelo. As massas dos órgãos segmentados foram comparadas com as da primeira versão. Informações sobre a massa ou o volume dos órgãos de diferentes linhagens de camundongos e, mais especificamente, da linhagem C57BL, também foram obtidas na literatura para comparação e para ajudar na segmentação. A imagem do camundongo representando uma fêmea da linhagem C57BL pesando 26 g foi gentilmente cedida pelo Turku Center for Disease e foi segmentada manualmente. O software GIMP® 2.10 foi usado para selecionar e segmentar cada órgão/tecido. O site IMAIOS-VET Anatomy foi usado como base anatômica para a identificação dos órgãos/tecidos. O software IMAGEJ® foi aplicado para montar as imagens segmentadas em uma pilha 3D e para converter as imagens segmentadas em arquivos binários. Os volumes dos órgãos segmentados foram medidos com um programa interno em C++. As densidades de tecido humano correspondentes fornecidas no ICRP 110 foram usadas para calcular a massa do órgão a partir dos volumes calculados. Os dados foram comparados com os relatórios da literatura. O número de órgãos segmentados aumentou de 20 no modelo antigo para 33 nos novos modelos. As massas dos órgãos segmentados neste trabalho, por diferentes pesquisadores, mostraram concordância na maioria dos casos. No entanto, órgãos como o intestino delgado, os ossos e a traquéia ainda merecem uma nova rodada de revisão.

Palavras-chave: dosimetria, phantoms de camundongos, modelo computacional, segmentação.

1 INTRODUCTION

Laboratory animals have been widely used in preclinical research to develop and testnew radiopharmaceuticals, therapeutic strategies and imaging techniques. They have also been used to investigate the dose-response relationship and the biological efficacy of different types of ionizing radiation. Biodistribution studies of new diagnostic radiopharmaceuticals are often conducted in murine in order to obtain a first estimate of absorbed doses in humans [19]. In this type of study, the absorbed doses in the animals rarely reach levels that can impair the results of the experiments [4].

However, some protocols may result in high absorbed doses in specific organs. Among such protocols, it is possible to include: i) longitudinal studies with extensive use of MicroCT and/or PET/SPECT images [23]; ii) research of therapy radiopharmaceuticals [26]; and iii) radiotherapy tests in small animals [2]. The precise quantification of absorbed doses and the determination of energy deposition patterns are of fundamental importance in the evaluation of biological effects in these types of experiments. Since such effects can even lead to biases, especially in longitudinal studies [14].

Physical measurement of absorbed doses in animal organs and tissues is not practical due to the invasiveness of these procedures. An alternative approach that has been successful in dosimetric evaluations is the use of computational models coupled with Monte Carlo (MC) codes for energy transport.

Several mouse models were developed in recent years and a good description of the history of the development of these phantoms can be found in the work of Mendes et al. (2017). Our group, in 2021, segmented and implemented a female mouse phantom of the C57BL strain called FM_BRA_01 for MCNP Monte Carlo Code [14].

In this work, a deep review of the segmentation of the mouse computational model FM_BRA_01 was carried out. In addition, new organs were identified and segmented for the improved version of the model. Two different researchers were responsible for segmenting the different organs in the model. The masses of the segmented organs of each researcher were compared among them and with the masses of the organs of the first version. The new models obtained were called FM_BRA_02 and FM_BRA_03.

2 METHODOLOGY

A high-resolution nuclear magnetic resonance (NMR) image of a female mouse of the C57BL/6 lineage was kindly provided by the Turku Center for Disease Modeling (TDCM, 2022).The Philips Achieva 3T equipment was used to acquire the whole body of the animal. Images were acquired using a three-dimensional gradient-echo sequence (3D-T1-FFE), with a spatial resolution of 0.138889 x 0.138889 x 0.16 mm^3 and with a matrix of 1280 x 720 x 181 voxels. In the first stage of this work, the original image was manipulated in order to prepare it for the segmentation process. The original DICOM image was opened in IMAGEJ®, converted to 8-bit and saved to a folder as a TIFF image sequence. Subsequently, to reduce the segmentation work, the number of images in the Z plane was reduced. Three images out of each set of four images were deleted. In this reduction, there is a loss of resolution in the Z axis and the voxel size becomes 0.14 x

0.14 x 0.64 mm^3. However, due care was taken to ensure that such a loss did not impair the identification and segmentation of the organs.

Then, using the "Crop" command, unnecessary parts of the images were removed, so that only the regions containing the animal's image were preserved. With such removal,

the 3D image matrix became 217x623x46 voxels. The segmentations of each organ/tissue of the animal were performed from this set of images.

The second stage of this work comprised the segmentation itself, i.e., the identification and attribution of a code or a color to the different tissues and organs of the animal. The GIMP®2.10 program (Fig. 1A) was used in this phase of the work. It is an open source program aimed mainly at creating and editing images, which allowed the selection and segmentation of organs/tissues from the 46 images. Segmentation was performed manually organ-by-organ. Free selection and contiguous selection tools were used to identify the organ (Fig. 1B). Once identified, the code <255>, white color, was assigned to the organ pixels and all the remaining pixels were assigned the value <0>, that is, black color (Fig. 1C). This procedure is called binarization. The fill tool, which assigns the selected area a color or texture, was used in this step. This procedure was repeated for each segmented organ or tissue, in all 46 images in the Z plane of the animal. The IMAIOS-VET Anatomy website (IMAIOS, 2022) has an interactive atlas of mouse anatomy based on CT images and was used as an anatomical basis to aid in the identification of organs/tissues.

Fig. 1: Example of kidney segmentation using the GIMP® software. A) Image of a Z plane (slice) loaded into the GIMP program. B) Kidneys identified. C) Segmented kidney.

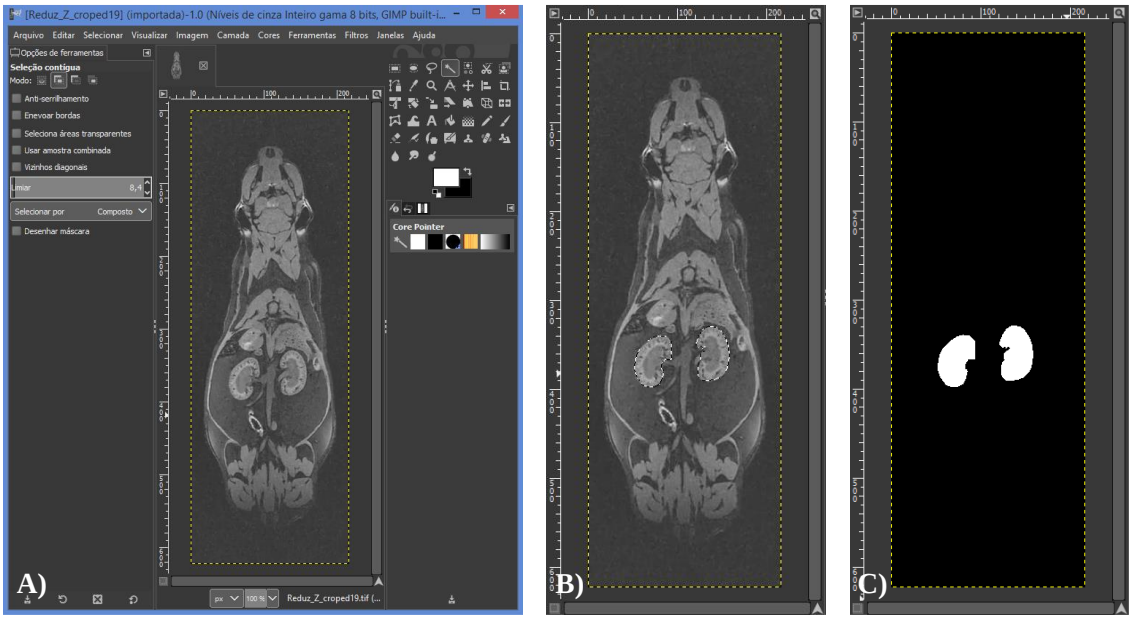

The contour of the animal's body was identified using the free selection tool and the contiguous selection tool, generating a tissue called “Whole Body”, comprising the entire volume of the mouse. This volume was used in the segmentation of the skin and the set of tissues called “Residual Tissues”. This block included all non-segmented tissues, especially adipose tissue, which is the main component of this set.

Still in the segmentation stage, the ImageJ® software was also used in the segmentation of the skin and in the identification of the content and wall of the organs of the digestive system and the urinary bladder. To perform the segmentation of these structures, the organ/tissue images were loaded into ImageJ®. The “erode” command was used to remove the outermost voxel layer from the images. The number of removed voxels varied according to the thickness of the skin or organ wall. These values were obtained from the literature and presented in Tab. 1. Considering the dimensions of the voxels in the X and Y two axes (0.15 mm) from 1 to 3 layers were removed, according to Tab. 1. After the erosion procedure, the eroded image corresponded to the contents of the organs (urine, feces, food bolus, etc.). The walls of the organs, as well as the skin, were obtained by subtracting the eroded image from the original image, using the ImageJ® command “ImageCalculator”.

Tab. 1: Literature data referring to the thickness of organs/tissues with wall and content and skin.

Organs	Thickness (mm)	References	# Outer layer voxel removed
Small intestine	0,25	[22]	2
Large intestine	0,15	[17]	1
Stomach	0,5	[10]	3
Bladder	0,025 a 0,040	[18]	1
Skin	0,204	[25]	1;2*

* - In FM_BRA_02, two voxels were removed from the outer layer and in FM_BRA_03, only one.

The last step of the segmentation consisted in the creation of “Residual Tissues”. For this purpose, all the images of the segmented organs were subtracted one-by-one from the “Whole Body” image using the ImageJ® command “ImageCalculator”.

An in house C^{++} program was used to calculate the volume of each segmented organ. To determine the organ masses, the density of the corresponding human tissues provided in ICRP 110 (ICRP, 2009) was used. For Harder's Gland, which is an organ that has no counterpart in human tissues, a density of 1.0 $g.cm^{-3}$ was assumed. The masses of

the organs segmented by each researcher were tabulated and compared with each other and with the masses of the original model (FM_BRA_01).

During segmentation, as mentioned earlier, the value <255> was assigned to the pixels of the segmented organs. The third step comprises assigning specific codes (different colors) to each organ/tissue. The IMAGEJ® software was used for this purpose. Each tissue has been assigned with a different code. For example, for the brain, the code 061 was set. Thus, in order for all pixels of the segmented images of the brain to have this value, a subtraction of <194> was performed in the segmented images of the brain (255 – 194 = 061). The command "Math ->Subtract" of ImageJ® was used for this purpose. This methodology was repeated for all organs segmented so that each one had a specific code, associated with a color in the image.

The last stage consisted in building a single 3D image, containing all the segmented organs, each with its specific code. Using the "ImageCalculator" command of the ImageJ® software, the segmented images with specific codes were added one-by-one. Two 3D models were obtained, one for each researcher. These new models were called FM_BRA_02 and FM_BRA_03. Amide® software was used to generate the color and rendered images of the completed models.

3 RESULTS

In these FM_BRA versions, each organ was segmented and composed of only one single volume and one single material. Coronal (Fig. 2A), sagittal (Fig. 2B) and transverse (Fig. 2C) sections of the FM_BRA_02 model are shown in Fig. 2. The rendering of the model (Fig. 2D) with some organs highlighted and the skeleton (Fig.1E) were also included. Specific colors were assigned to each segmented organ. Thirty-four organs/tissues were segmented, compared to the 21 organs and tissues segmented in the old model, FM_BRA_01. The complete list of organs, as well as their respective masses, can be seen in Tab. 2.

Fig. 1 - Graphic representations of the FM_BRA model obtained through the AMIDE® software. Coronal (A) Sagittal (B) and cross sections (C). 3D rendering of the whole body, with kidney, adrenal glands, uterus and bladder highlighted (D). Skeleton 3D rendering (E)

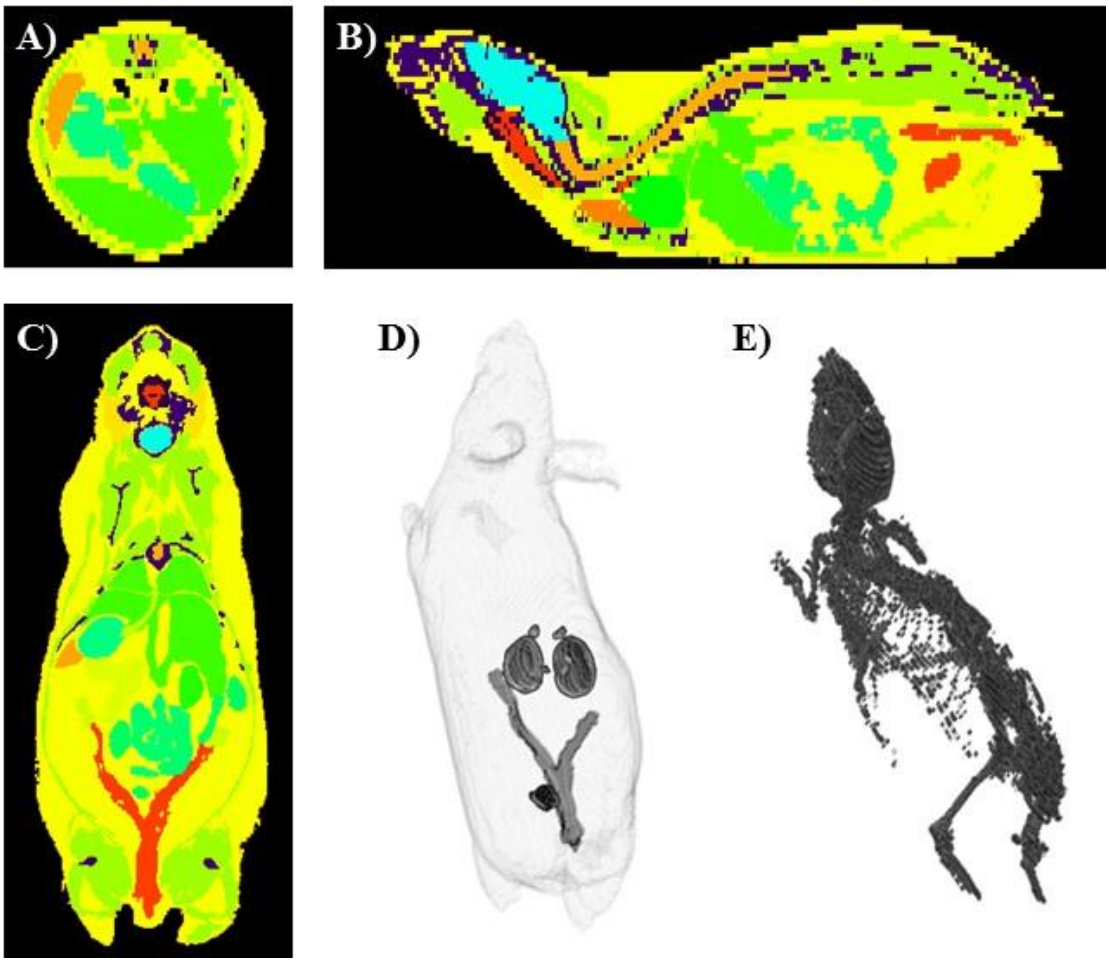

All versions of the model showed significant mass differences when compared to each other. The minimum and maximum differences between the original version (FM_BRA_01) and the FM_BRA_02 version of this work were -79% and 342% respectively.

Tab. 2: Density and mass of segmented organs and tissues in mouse models FM_BRA_01, FM_BRA_02 and FM_BRA_03 and comparisons among the models.

Organs	ρ (g.cm^{-3})	Mass (g)			Differences among the models		
		FM_BRA 01	FM_BRA 02	FM_BRA 03	FM_BRA 02 vs 01	FM_BRA 03 vs 01	FM_BRA 03 vs 02
Spleen	1,04	0,079	0,110	0,096	-28%	-18%	-12%
Bladder - Wall	1,04	-	-	0,009	-	-	-
Bladder - Content	1,04	-	-	0,020	-	-	-
Bladder	1,04	0,026	0,027	0,029	-4%	-12%	9%
Brain	1,05	0,382	0,455	0,447	-16%	-14%	-2%
Heart	1,05	0,270	0,296	0,281	-9%	-4%	-5%
Esophagus	1,04	-	-	0,039	-	-	-
Stomach - Wall	1,04	-	-	0,097	-	-	-

Stomach - Content	1,04	-	-	0,100	-	-	-
Stomach	1,04	0,158	0,177	0,197	-11%	-20%	11%
Liver	1,05	1,680	2,239	1,855	-25%	-9%	-17%
G. Right suprarenal.	1,03	-	0,004	-	-	-	-
G. Left suprarenal.	1,03	-	0,004	-	-	-	-
G. adrenal	1,03	-	0,007	0,005	-	-	-28%
Harder's Gland	1,00	-	0,035	0,030	-	-	-14%
Salivary glands	1,03	0,194	0,165	0,192	18%	1%	16%
Small Intestine - Wall	1,04	-	-	0,497	-	-	-
Small Intestine - Contents	1,04	-	-	0,459	-	-	-
Small intestine	1,04	-	0,670	0,956	-	-	43%
Large Intestine - Wall	1,04	-	-	0,282	-	-	-
Large Intestine - Contents	1,04	-	-	0,468	-	-	-
Large intestine	1,04	-	0,927	0,750	-	-	-19%
intestines	1,04		1,597	1,706	-	-	7%
Spinal cord	1,03	0,091	0,136	0,121	-33%	-25%	-11%
muscles	1,05	5,197	6,616	7,650	-21%	-32%	16%
Eyes - Bulb	1,05	-	-	0,022	-	-	-
Eyes - Crystalline	1,05	-	-	0,004	-	-	-
Right eye	1,05	-	0,016	-	-	-	-
Left eye	1,05	-	0,012	-	-	-	-
Eyes	1,05	0,006	0,028	0,026	-79%	-77%	-8%
bones	1,04	0,873	1,310	2,701	-33%	-68%	106%
ovaries	1,04	-	-	0,017	-	-	-
pancreas	1,05	0,155	0,232	0,237	-33%	-35%	2%
Skin	1,09	-	1,732	1,170	-	-	-32%
Lung	0,38	0,161	0,220	0,185	-27%	-13%	-16%
left kidney	1,05	-	0,169	0,158	-	-	-6%
Right Kidney	1,05	-	0,157	0,168	-	-	7%
Kidneys	1,05	0,282	0,326	0,326	-13%	-14%	0%
thymus	1,03	-	0,075	0,065	-	-	-13%
Thyroid	1,04	0,084	0,019	0,017	342%	404%	-12%
Trachea	1,03	-	0,094	0,064	-	-	-32%
Uterus	1,03	0,125	0,117	0,129	7%	-3%	10%
Gallbladder	1,03	-	-	0,016	-	-	-
Waste Tissues	0,95	-	-	15,507	-	-	-

Similarly, when the organ mass values of the FM_BRA_01 model were compared with the values of the FM_BRA_03 model, the minimum and maximum differences were -77% and 404%. The organs that presented these differences were eyes and thyroid, indicating that some segmentation problem may have occurred with these organs.

The comparison FM_BRA_02 vs FM_BRA_03 showed smaller differences. For most organs, discrepancies were less than ± 15%. However, for the organs/tissues “Bone”, “Small Intestine”, “Trachea” and “Skin” the differences were significant: 106%, 43%, -32% and -32%, respectively. Bones and trachea are organs that are difficult to segment on NMR images, as the low signal of this tissue results in dark regions with borders that are difficult to define. Furthermore, these are organs with very complex

geometry, as well as the small intestine, which makes segmentation challenging. In the case of skin, the variation was expected and resulted from the choice of the researchers responsible for the segmentation for different thicknesses: FM_BRA_02 (1 voxel thick) and FM_BRA_03 (2 voxel thick).

The masses of organs and tissues segmented in the FM_BRA_02 and FM_BRA_03 models were also compared with the masses of organs and tissues in mice reported by other authors [15]; [14]; [16]; [27]; [3]; [20]; [11]; [13]; [1]; [6]; [19]. This comparison can be seen in Table 3.

Tab. 3: Comparison between the mass values of the organs segmented in this work and the minimum, maximum and average values of the respective mouse organs obtained in the literature.

Organ Mass (g)	FM_BRA_02	FM_BRA_03	Values obtained from data presented in the literature *		
			Average	Min	Max
Spleen	0,110	0,096	0,128	0,022	0,216
Bladder	0,027	0,029	0,112	0,012	0,238
Brain	0,455	0,447	0,501	0,350	0,635
Heart	0,296	0,281	0,207	0,115	0,290
Stomach	0,177	0,197	0,273	0,175	0,438
Liver	2,239	1,855	1,820	0,780	2,690
E. Adrenal	0,007	0,005	0,007	0,004	0,011
intestine	1,597	1,706	2,297	0,952	2,941
Spinal cord	0,136	0,121	0,112	0,048	0,190
Muscle	6,616	7,650	14,686	12,254	17,117
Eyes	0,028	0,026	0,005	0,004	0,006
bones	1,310	2,701	1,936	0,110	3,336
pancreas	0,232	0,237	0,193	0,041	0,440
Skin	1,732	1,170	4,326	2,228	6,910
Lung	0,220	0,185	0,127	0,096	0,167
Kidneys	0,326	0,326	0,407	0,265	0,586
Thyroid	0,019	0,017	0,030	0,005	0,105

* - [15]; [14]; [16]; [27]; [3]; [20]; [11]; [13]; [1]; [6]; [19].

As can be seen in Table 3, the mass values of most organs and tissues segmented in this work are within the limits reported by other authors. The exceptions were: muscle and skin, whose masses were smaller than those reported in the literature; and eyes and lung, with larger masses. In the case of muscle mass, many authors include all unidentified tissues in that tissue. In our work, we did not adopt this practice and this may be the reason for the discrepancy observed for this organ. In the case of the skin, eyes and lung, a review of the segmentation is necessary to confirm whether the masses obtained

for these organs are correct and are based on the anatomical variation of C57BL/6strain or whether there has been an inaccuracy in the segmentation.

It should also be mentioned that the wall thickness of the urinary bladder in this work, 0.15 mm, is considerably greater than that reported by Schuethet al. (2018): 0.025 to 0.040 mm [18]. This fact occurred due to the typical limitation of voxel models for segmentation of thin-walled organs: the lowest possible thickness corresponds to the voxel dimension and the decrease in voxel dimensions results in more work in the segmentation and increased computational time when the model is used in Monte Carlo calculations.

4 CONCLUSION

The voxelized mouse model FM_BRA_01 was revised and improved by two different researchers and two new models were generated: FM_BRA_02 and FM_BRA_03. All organs of the original model were re-segmented. The total number of segmented organs and tissues increased from 20 in the old model to 33 in the new models. It was possible to differentiate the organ wall and content for the bladder, stomach, large intestine and small intestine.

The masses of the organs segmented in this work, by the different researchers, showed agreement in most cases. However, organs such as the small intestines, bones and trachea still deserve a new round of review, as they showed significant discrepancies between the two segmentations performed in this study. It was possible to observe that the segmentations of certain organs such as bones, intestines and trachea, present a higher level of difficulty in relation to other organs such as brain, heart and liver. The most significant mass differences were observed for these organs and varied considerably according to the experience of each researcher responsible for the segmentation process.

The comparison of the masses of the organs segmented in this work with data reported by other researchers also allowed the identification that the segmentation of the eyes, skin, muscle and lungs must undergo a review in the future. This should be achieved to determine whether the masses obtained for these organs are correct and are part of the anatomical variation of this strain (C57BL/6) or if further corrections are necessary.

REFERENCES

[1] A. Bitar,;*et al.* Avoxel-based mouse for internal dose calculations using Monte Carlo simulations (MCNP). *Phys. Med. Biol.*,v.52, p.1013-1025, (2007).

[2] E.R, Biglin,;*et al.* Dosimetriapré-clínica: explorando o uso de simuladores de pequenosanimais. *Radiat Oncol* 14**,** 134 (2019). https://doi.org/10.1186/s13014-019-1343-8.

[3] S. Boutaleb,;*et al.* Impact of mouse model on preclinical dosimetry in targeted radionuclide therapy. Proc. IEEE, v.97, p.2076-2085, (2009).

[4] S.K. Carlson,:*et al.*"Small animal absorbedradiation dose from serial micro-computed tomography imaging". *Mol. Imaging Biol.*, v.9, p.78-82, (2007).

[5] A. Flynn,:*et al.* A mouse model for calculating the absorbed beta-particle dose from131I- and 90Y-labeled immunoconjugates, including a method for dealing with heterogeneity in kidney and tumor. Radiat. Res., v.156, p.28-35, (2001).

[6] C. Hindorf,; M. L. Jungberg,; S.E. Strand, Evaluation of parameters influencing S values in mouse dosimetry. J. Nucl. Med., v.45, p.1960-1965, (2004).

[7] T. E. Hui,:*et al*. A mouse model for calculating cross-organ beta doses from yttrium-90-labeled immune conjugates. Cancer, v.73, n.3, suppl., p.951-957, (1994)

[8] INTERNATIONAL COMISSION ON RADIOLOGICAL PROTECTION. ICRP. Adult reference computational phantoms. Oxford: Pergamon Press, 2009. (ICRP Publication, 110).

[9] IMAIOS (Medical and e-learning websites for healthcare professionals). "WholeBody – Mouse – CT", em: https://www.imaios.com/en/vet-Anatomy/Mouse/Mouse-Whole-body-CT, acessado em Agosto de 2022.

[10] W. Kang,; L. Maher,; M. Michaud,; *et al.* Development of a Novel Orthotopic Gastric Cancer Mouse Model. *BiolProced Online* 23**,** 1 (2021). https://doi.org/10.1186/s12575-020-00137-1

[11] M.A. Keenan,;*et al.* Realistic animal model series for dose assessment. *J. Nucl. Med.*, v.51, n.3, p.471-476, (2010).

[12] K.S. Kolbert,;*et al.* Murine S factors for liver, spleen, and kidney. *J. Nucl. Med.*, v.44, n.5, p.784- 791,(2003).

[13] T. Mauxion,;*et al*. Improved realism of hybrid mouse models may not be sufficient to generate reference dosimetric data. *Med. Phys.*, v.40, n.5, p.1-13, (2013).

[14] B. M. Mendes,; *et al.* Development of a mouse computational model for MCNPx based on Digimouse® images and dosimetric assays. *Brazilian Journal of Pharmaceutica lSciences.* http://dx.doi.org/10.1590/s2175-97902017000116092. (2017).

[15] W. H. Miller,; *et al.* Evaluation of beta-absorbed fractions in a mouse model for 90Y, 188Re, 166Ho, 149Pm, 64Cu, and 177Lu radionuclides. Cancer Bio0therRadiopharm. (2005) Aug;20(4):436-49. doi: 10.1089/cbr.2005.20.436. PMID: 16114992.

[16] A. Mohammadi and S. Kinase. Influence of voxel size on specific absorbed fractions and S-values in a mouse voxel phantom. *Radiat. Prot. Dosim.*, v.143, n.2/4, p.258-263, 2011.

[17] P. Paone,;*et al.* Mucus barrier, mucins and gut microbiota: the expected slimy partners? Gut. (2020) Vol. 69 (12) p.2232-2243. doi: 10.1136/gutjnl-2020-322260.

[18] A. Schueth,;*et al.* (2018*). High-resolution bladder morphology in the intact mouse bladder: an intravital two-photon study. Cold Spring Harbor Laboratory - bioRxiv*.https://doi.org/10.1101/508879

[19] M. G. Stabin,**;** *et al.* Voxel-based mouse and ratmodels for internal dose calculations. *J. Nucl. Med.*, v.47, n.4, p.655- 659, (2006).

[20] R. Taschereau and A, F. Chatziioannou. Monte Carlo simulations of absorbed dose in a mouse phantom from 18-fluorine compounds. Med. Phys., v.34, n.3, p.1026- 1036, (2007).

[21] TDCM (Turku Center for Disease Modeling). “Magnetic Resonance Imaging”, em:https://www.tcdm.fi/services/animal-imaging-unit/magnetic-resonance-imaging/, acessado em agosto de 2022.

[22] B. P. Vazquez,; *et al.* Inflammatory responses and intestinal injury development during acute *Trypanosomacruzi* infection are associated with the parasite load. Parasites Vectors 8**,** 206 (2015). https://doi.org/10.1186/s13071-015-0811-8.

[23] K. Veerle,:*et al.*Micro-CT for anatomic referencing in PET and SPECT: Radiation dose, biologic damage, and image quality. *Journal of nuclear medicine: official publication, Society of Nuclear Medicine.* (2011). v.52. (11)p.1827-1833. 10.2967/jnumed.111.089151.

[24] G. J. Wang and L. Cai. Induction of cell-proliferation hormesis and cell-survival adaptive response in mouse hematopoietic cells by whole-body low-dose radiation. Toxicol. Sci., v.53, p.369-376, (2000).

[25] J. C J. Wei,:*et al.* Allometric scaling of skin thickness, elasticity, visco elasticity to mass for micro-medical device translation: from mice, rats, rabbits, pigs to humans. *Sci Rep* 7**,** 15885 (2017). https://doi.org/10.1038/s41598-017-15830-7.

[26] M. Yonezawa, Induction of radio-resistance by low dose X-irradiation. Yakugaku Zasshi, v.126, n.10, p.833-840, (2006).

[27] X, Zhang,; *et al.* Organ dose conversion coefficients based on a voxel mouse model and MCNP code for external photon irradiation. Radiat. Prot. Dosim., v.148, n.1, p.9-19, 2012.